Journal of Power Sources 196 (2011) 7874–7877

Contents lists available at ScienceDirect

Journal of Power Sources

journal homepage: www.elsevier.com/locate/jpowsour

Short communication

Supercapacitors incorporating hollow cobalt sulfide hexagonal nanosheets

Zusing Yang, Chia-Ying Chen, Huan-Tsung Chang*

Department of Chemistry, National Taiwan University, 1, Section 4, Roosevelt Road, Taipei 106, Taiwan

ARTICLE INFO

Article history:
Received 26 November 2010
Received in revised form 1 March 2011
Accepted 28 March 2011
Available online 6 April 2011

Keywords:
Supercapacitors
Nanomaterials
Energy storage
Electrode materials

ABSTRACT

We have prepared hollow cobalt sulfide (CoS) hexagonal nanosheets (HNSs) from $Co(NO_3)_2$ and thioacetamide in the presence of poly(vinylpyrrolidone) (PVP) at 100 °C under alkaline condition. The as-prepared hollow CoS HNSs have an average edge length ca. 110 ± 27 nm and an outer shell of 16 ± 4 nm in thickness from 500 counts. The CoS HNSs are deposited onto transparent fluorine-doped tin oxide (FTO) substrates through a drop-dry process to prepare two types of supercapacitors (SCs); high rate and large per-area capacitance. The electrolyte used in this study is $KOH_{(aq)}$. The CoS HNSs (8 μg cm^{-2}) electrodes exhibit excellent capacity properties, including high energy density (13.2 h kg^{-1}), power density (17.5 kW kg^{-1}), energy deliverable efficiency (81.3–85.3%), and stable cycle life (over 10,000 cycles) at a high discharge current density of 64.6 A g^{-1}. With their fast charging and discharging rates (<3 s), the CoS HNSs show characteristics of high-rate SCs. The CoS HNS SCs having high mass loading (9.7 mg cm^{-2}) provide high per-area capacitance of 1.35 F cm^{-2} and per-mass capacitance of 138 F g^{-1}, respectively, showing characteristics of SCs with large per-area capacitance. Our results have demonstrated the potential of the CoS HNS electrodes hold great practical potential in many fields such as automobile and computer industries.

1. Introduction

Developing cheap, effective, and environmentally friendly renewable energy storage [1] and conversion devices will be essential for satisfying future energy needs [2]. Electrochemical capacitors, also known as supercapacitors (SCs) or ultracapacitors, are powerful energy storage systems that fill the gap between batteries and conventional capacitors [3]. The charging and discharging of SCs are faster processes than those of conventional capacitors (occurring within a few seconds), leading to higher power delivery or uptake. With their advantageous properties (large surface sizes, excellent capacitances, low toxicities, and low cost), several nanomaterials, including carbon nanotubes (CNTs) [4], Fe_3O_4 nanoparticles (NPs) [5], MnO_2 NPs [6], and $Ni(OH)_2$ nanoplates [7], have been developed as SCs. Nevertheless, high-rate SCs exhibiting high power densities (>15 kW kg^{-1}) and long cycle lives (>10,000 cycles) have not been realized. To do so will require the preparation of materials that allow the generation of high current densities (>40 A g^{-1}) within rapid discharge times (<3 s) [8,9].

Batteries or fuel cells incorporating high-power SCs are ideal hybrid power sources that can be applied in many fields, especially in the automobile industry, where the SCs provide peak power during conjuncture acceleration and become recharged during braking, and where the batteries or fuel cells provide the necessary energy for the vehicle [10,11]. Ideal SCs acting as primary power sources require short-term (high-rate) power boosts; several attempts have been made to prepare such systems using nanostructures of various shapes [7,9,12,13], but with limited success [9]. In those few cases, organic binders (adhesives), such as poly(tetrafluoroethylene) (PTFE), were used to attach the nanostructures to the surfaces of the conducting substrates; the presence of these binders had a negative impact on the flow of ions during the redox reactions at the interfaces between the nanomaterials and the electrolytes, leading to decreased capacitance [14].

In this study, we prepared hollow cobalt sulfide (CoS) hexagonal nanosheets (HNSs) from $Co(OH)_2$ and thioacetamide through a hydrothermal process, performed under alkaline conditions, using polyvinylpyrrolidone (PVP) as a stabilizer. To fabricate stable and efficient SCs, we deposited the as-prepared hollow CoS HNSs onto fluorine-doped tin oxide (FTO) substrates. $KOH_{(aq)}$ was used as an electrolyte. The as-prepared CoS HNS SCs provided high values of specific capacitance (C), energy density (E), and power density (P), with extremely short discharge times (<3 s) and high stability (>10,000 cycles).

2. Experimental

2.1. Materials

Commercially available cobalt nitrate, EtOH, Nafion, KOH, PVP (M_w 55,000), NaOH, and thioacetamide were purchased from Sigma–Aldrich (Milwaukee, WI, USA).

* Corresponding author. Tel.: +11 886 2 33661171; fax: +11 886 2 33661171.
E-mail address: changht@ntu.edu.tw (H.-T. Chang).

0378-7753/$ – see front matter © 2011 Elsevier B.V. All rights reserved.
doi:10.1016/j.jpowsour.2011.03.072

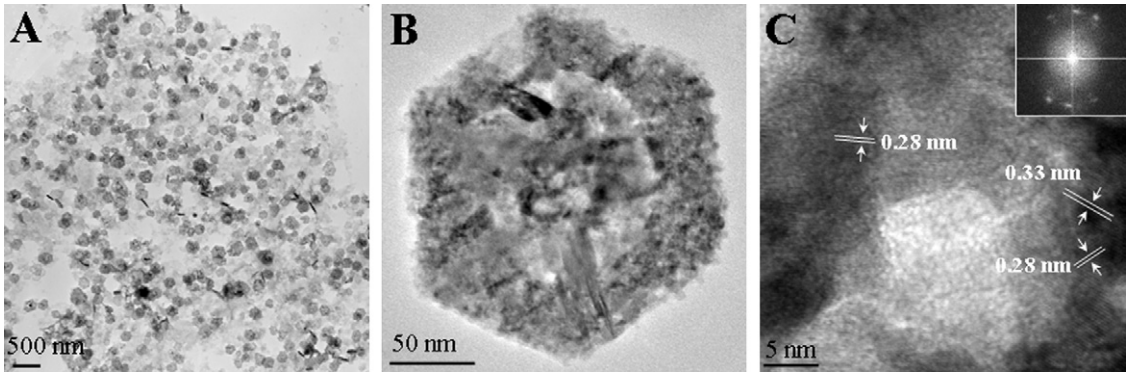

Fig. 1. (A) TEM images of CoS HNSs. (B, C) High-magnitude (B) TEM and HRTEM images of an individual hollow CoS HNS. Inset to (C): Corresponding FFT pattern.

2.2. Preparation of hollow CoS HNSs

$Co(NO_3)_2$ (0.291 g), thioacetamide (0.15 g), and PVP (0.07 g) were added to ultrapure H_2O (final volume: 50 mL) in a glass bottle. After addition of 0.5 M NaOH (12 mL), the solution was heated at 100 °C for 60 min. The color changed from aquamarine to black, indicating the formation of CoS HNSs. The CoS HNSs solution was subjected to sonication for at least 60 min and then to two centrifugation (10,000 rpm, 10 min)/wash (EtOH, 1.5 mL) cycles. The CoS HNSs were then re-dispersed in EtOH (1.0 mL) prior to use.

2.3. Preparation of CoS HNS electrodes

Drops (5 μL) of the dispersed CoS HNS solution (0.8 mg in 1 mL of EtOH) were placed on the FTO surfaces, each having an effective area of 1 cm^2 [15]. The substrates were then dried in an oven at 100 °C for 10 min. FTO substrates were employed in this study, mainly because: (1) it is a commercial available conducting glass; (2) its effective area of FTO relative to that of glassy carbon electrode can be easily controlled; and (3) it has strong interaction with the as-prepared CoS HNSs, preventing adding any of adhesives.

2.4. Preparation of large-area capacitive SCs

The preparation of large-area capacitive SCs featuring CoS HNSs was similar to that for the preparation of CoS HNS electrodes, except for use of a different amount of CoS HNSs (9.7 mg). Prior to electrochemical testing, the as-prepared SCs were covered with a solution of Nafion in EtOH (0.5%, 10 μL) to prevent the release of CoS HNSs from the surface.

2.5. Measurements

Transmission electron microscopy (TEM) images were recorded using a JEOL JSM-1230 instrument (Hitachi, Tokyo, Japan). A Tecnai 20 G2 S-Twin TEM system (Philips, OR, USA) was used to record high-resolution TEM (HR-TEM) images. Cyclic voltammetry (CV), impedance, and galvanostatic charge/discharge tests were performed using a CHI 700D electrochemical analyzer (CH Instruments, Austin, TX). All measurements were performed using 1 M KOH as the electrolyte. CV measurements of the CoS HNS electrodes (effective area: 1.0 cm × 1.0 cm) were performed using a three-electrode system: a HNS electrode as a working electrode, a Pt counter electrode, and a saturated calomel electrode (SCE) reference electrode. Impedance data were collected at an applied potential of 0 V over the frequency range from 100 kHz to 0.1 Hz. Galvanostatic charge/discharge tests were performed over a potential range from 0 to 0.6 V at a constant discharge current density of 64.6 A g^{-1}.

3. Results and discussion

3.1. Preparation of CoS HNS electrodes

Hexagonal shaped β-$Co(OH)_2$, is a precursor for the preparation of CoS HNSs, which is similar to that for the preparation of two-dimensional Co_3O_4 nanostructures, including NSs, nanowalls, and nanoplates [16–18]. To prepare stable β-$Co(OH)_2$, we added NaOH to Co^{2+} aqueous solution in the presence of PVP. The as-prepared β-$Co(OH)_2$ precursors then reacted with S^{2-} ions that was produced from thermal decomposition of thioacetamide at 100 °C to form CoS HNS in Fig. 1A. The formation mechanism of CoS HNS is based on the follow reactions:

$$Co^{2+} + 2OH^- \rightarrow Co(OH)_{2(s)} \quad \text{(aquamarine color)} \tag{1}$$

$$Co(OH)_{2(s)} + S^{2-} \rightarrow CoS_{(s)} \quad \text{(black color)} + 2OH^- \tag{2}$$

We observed no products or precipitates in the absence of NaOH, revealing the important role of the $Co(OH)_2$ precursors in the formation of the product. The product had an average edge length of 110 ± 27 nm and an outer shell having a thickness of 16 ± 4 nm (500 counts). Fig. 1B displays a representative high-magnification TEM image of a product. Detailed structural analyses from the *d*-spacing and the fast Fourier transform (FFT) pattern (Fig. 1C) revealed a set of (220) planes having a lattice spacing of 0.33 nm and a set of (3 1 1) planes, each with a lattice spacing of 0.28 nm, in the hollow product. Energy dispersive X-ray (EDX) spectroscopic analysis revealed the existence of cobalt and sulfur atoms (Fig. S1) in the as-prepared product, revealing that the product is CoS HNSs. X-ray photoelectron spectroscopy (XPS) data confirmed the existence of sulfur (Fig. S2).

We used the as-prepared hollow CoS HNSs to prepare CoS HNS electrodes on FTO substrates without employing any additional current collectors (e.g., conducting graphite) or adhesives (e.g., PTFE) [19]. PVP served not only as a stabilizer in the synthesis of the CoS HNSs but also as a current collector and adhesive in the as-prepared CoS HNS electrodes. Fig. S3A displays photographs of a representative FTO substrate before and after deposition of the CoS HNSs; the intense black color in the latter image supports the successful deposition of the CoS HNSs. The top-view SEM image (Fig. S3B) reveals that the FTO substrate was covered with aggregated CoS HNSs. The inset to Fig. S3B provides a magnified SEM image of the as-prepared CoS HNSs; from it, we estimated the thickness of the CoS HNSs to be ca. 100 nm.

3.2. High-rate SCs

Fig. 2A presents CV curves of a representative CoS HNS electrode tested at various scan rates (from 10 to 100 mV s^{-1}). These CV curves are not the rectangular shapes typically observed for

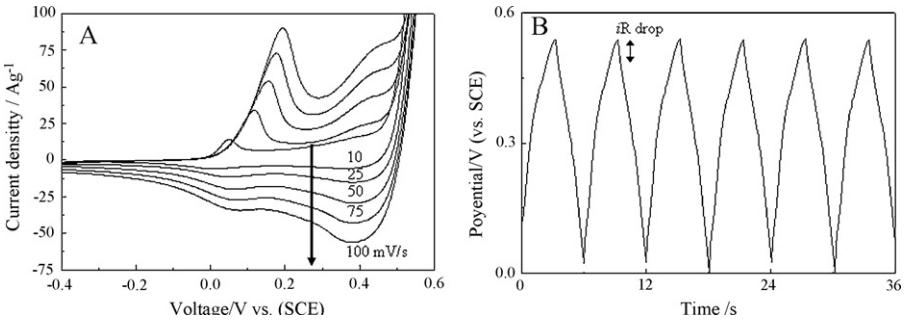

Fig. 2. (A) CV curves of a representative CoS HNS electrode, recorded at various scan rates. (B) Galvanostatic charge/discharge curves of the CoS HNS electrode, recorded at a constant current density of 64.6 A g^{-1}.

ideal electric double-layer capacitors; indeed, the as-prepared CoS HNS electrode exhibited pseudocapacitive characteristics [13,19], which resulted from reversible electrochemical redox reactions [13,19]. Although the mechanism of these reactions is not well understood, it appears to be similar to that of $Co(OH)_2$, based on the similar redox peak potentials and the similar profiles of the CV curves recorded using KOH as the electrolyte, and the sulfur and oxygen are belong to the same group [13,19–21]. According to the literatures [13,19], the two anodic peaks (Fig. 2A) are likely due to the oxidations of CoS to CoSOH and CoSOH to CoSO, separately:

$$CoS + OH^- \leftrightharpoons CoSOH + H_2O + e^- \quad (3)$$

$$CoSOH + OH^- \leftrightharpoons CoSO + H_2O + e^- \quad (4)$$

The two oxidized peaks of the as-prepared CoS nanomaterials occur separatelty at the voltages 0.1–0.2 and 0.3–0.4, which are different from those (0.2 and 0.5 V) for $Co(OH)_2$ nanomaterials [21]. Next, we conducted galvanostatic charge/discharge tests to obtain the values of C, E, and P of the CoS HNS electrode. Fig. 2B presents the galvanostatic charge/discharge curves of the electrode, recorded at a constant discharging current density of 64.6 A g^{-1}. We calculated the values of C of the SCs from the galvanostatic discharge curves according to the equation:

$$C = i \times \Delta t(\Delta V \times m) \quad (5)$$

where i is the discharging current (A), Δt is discharge time (s), ΔV is the potential drop (V) during discharge after the internal resistance (iR) drop, and m is the mass (g) of the CoS HNSs on the electrode. In 1 M KOH as the electrolyte and at a high discharge current density of 64.6 A g^{-1}, the average value (five repetitive measurements) of C was ca. 326.4 F g^{-1}. We then calculated the average values of E and P for the CoS HNS electrode using the equations [22,23]

$$E = \frac{0.5C(\Delta V)^2}{3.6} \quad (6)$$

and

$$P = \frac{E}{\Delta t} \quad (7)$$

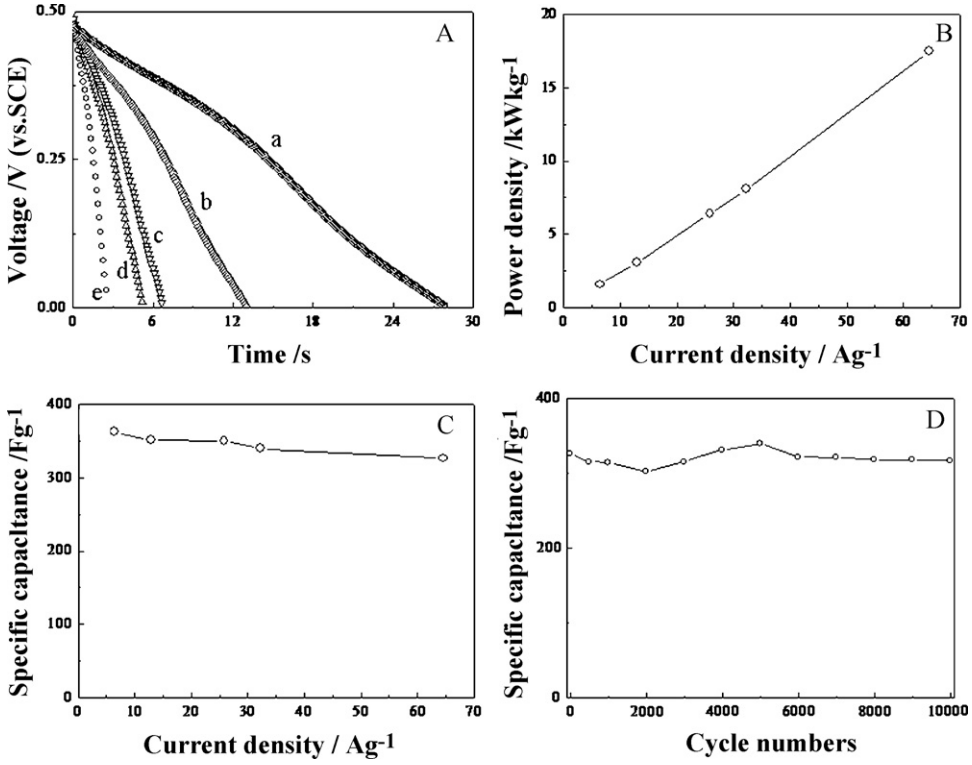

Fig. 3. (A) Galvanostatic discharge curves of the CoS HNS electrode, recorded at current densities of (a) 6.46, (b) 12.92, (c) 25.84, (d) 32.30, and (e) 64.60 A g^{-1}. (B) Power densities of the CoS HNS electrode, recorded at various applied current densities. (C) Specific capacitances of the CoS HNS electrode, recorded at various applied current densities. (D) Specific capacitance of the CoS HNS electrode in 1 M KOH, plotted with respect to the number of charge/discharge cycles.

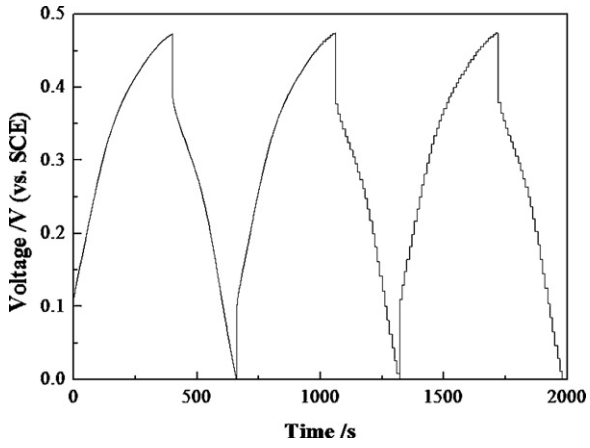

Fig. 4. Galvanostatic charge/discharge curves of a representative large-area capacitive CoS HNS electrode.

obtaining values of ca. 13.2 Wh kg^{-1} and 17.5 kW kg^{-1}, respectively. These values are both larger than those of carbon-based double-layer capacitors (E = ca. 5 Wh kg^{-1}; P = ca. 10 kW kg^{-1}) [1], multilayer CNT-based SCs (P = ca. 7 kW kg^{-1}) [15], graphene-based SCs (P = ca. 10 kW kg^{-1}) [24], and Au/Ag SCs (E = ca. 2.4 Wh kg^{-1}; P = ca. 12 kW kg^{-1}) [25]. Notably, the CoS HNS electrodes provided an average value of P that satisfied the power target (15 kW kg^{-1}) of the Partnership for New Generation of Vehicles (PNGV) at a fast power delivery rate (discharge time <3 s) [8,9]. Our results clearly show that the CoS HNSs are excellent nanomaterials for fabrication of high-rate SCs.

The galvanostatic discharge curves of the CoS HNS electrodes, recorded at various current densities (Fig. 3A), revealed that they exhibited rapid discharge capability, even at a low current density of 6.46 A g^{-1} (<30 min). The value of C at a high current density (64.6 A g^{-1}) was ca. 90% of that at the low current density (6.46 A g^{-1}), revealing excellent cycling characteristics (Fig. 3B). Fig. 3C indicates that the value of P increased from 1.58 to 17.5 kW kg^{-1} upon increasing the discharge current density from 6.46 to 64.6 A g^{-1}. We tested the cycle life and the energy deliverable efficiency (η) of the CoS HNS electrodes by performing continuous charge/discharge cycles (up to 10,000 cycles) at a constant discharge current density of 64.6 A g^{-1} (Fig. 3D). Using the equation [15]:

$$\eta = \left(\frac{t_d}{t_c}\right) \times 100\% \quad (8)$$

where t_d and t_c are the discharge and charge times, respectively, we calculated values of η of 81.4 and 85.3% for the first and 10,000th cycles, respectively. The loss in the value of C after 10,000 cycles was only ca. 2.8% relative to that obtained from the first cycle, confirming the excellent electrochemical stability of the CoS HNS electrode. We suspect that the enhancement in the value of η and the slight decrease in the value of C after 10,000 cycles were due primarily to the stable equilibrium between the electrolyte and the CoS HNSs.

3.3. Large per-area capacitance

SCs having relatively high specific capacitances (>100 F g^{-1}) usually provide very low mass loading (mF cm^{-2} level). To further demonstrate the novel applicability of these effective CoS HNS electrodes, we used them to fabricate SCs providing large per-area capacitance. Fig. 4 reveals that the CoS HNSs (mass loading: 9.7 mg; effective area: 1 cm^2) on FTO substrates provided a capacitance per area of 1.35 F cm^{-2}, comparable with that (1.2 F cm^{-2}) of carbon-based SCs (60 mg cm^{-2}) [26]. We also noted the SCs incorporating CoS HNSs (9.7 mg cm^{-2}) exhibited C, E and P values of 138 F g^{-1}, 4.3 Wh kg^{-1}, and 0.06 kW kg^{-1} at a discharge current of 2 mA cm^{-2}, respectively. Therefore, we suspect that our CoS HNSs are superior over most of the reported SCs [6,26].

4. Conclusions

In conclusion, we have prepared CoS HNSs and employed them as SCs. The SCs featuring CoS HNSs provided high values of C (326.4 F g^{-1}), E (13.2 Wh kg^{-1}), and P (17.5 kW kg^{-1}) at a high current density (64.6 A g^{-1}). After performing 10,000 charge/discharge cycles, the SCs featuring the CoS HNSs exhibited a value of η of 85.4% and only a slight decrease in the value of C (2.8%). Relative to widely used MnO_2 and graphene-based SCs, our CoS HNS SCs provided a higher capacitance and a longer cycle life. In addition, CoS HNS SCs having high mass loading (9.7 mg cm^{-2}) provided high per-area capacitance of 1.35 F cm^{-2} and per-mass capacitance of 138 F g^{-1}, suggesting that they have great practical potential for use as energy sources in computer and automobile products.

Acknowledgments

We thank the National Science Council, Taiwan, for financial support (NSC 98-2113-M-002-011-MY3, 99-2627-M-002-016, and 99-2627-M-002-017). Z.Y. thanks the National Taiwan University for the award of a postdoctoral fellowship in the Department of Chemistry, National Taiwan University.

Appendix A. Supplementary data

Supplementary data associated with this article can be found, in the online version, at doi:10.1016/j.jpowsour.2011.03.072.

References

[1] B.E. Conway, Electrochemical Supercapacitors, Kluwer Academic/Plenum Publisher, New York, 1999.
[2] M.C. Hanna, A.J. Nozik, J. Appl. Phys. 100 (2006) 074510–074518.
[3] P. Simon, Y. Gogotsi, Nat. Mater. 7 (2008) 845–846.
[4] D.N. Futaba, K. Hata, T. Yamada, T. Hiraoka, Y. Hayamizu, Y. Kakudate, O. Tanaike, H. Hatori, M. Yumura, S. Iijima, Nat. Mater. 5 (2006) 987–994.
[5] N.-L. Wu, S.-Y. Wang, C.-Y. Han, D.-S. Wu, L.-R. Shiue, J. Power Sources 113 (2003) 173–178.
[6] A.E. Fisher, K.A. Pettigrew, D.R. Rolison, R.M. Stroud, J.W. Long, Nano Lett. 7 (2007) 281–286.
[7] H. Wang, H.S. Casalongue, Y. Liang, H. Dai, J. Am. Chem. Soc. 132 (2010) 7472–7477.
[8] B. Scrosati, Nature 373 (1995) 557–558.
[9] D.-W. Wang, F. Li, M. Liu, G.Q. Lu, H.-M. Cheng, Angew. Chem. Int. Ed. 47 (2008) 373–376.
[10] A. Burke, J. Power Sources 91 (2000) 37–50.
[11] R. Kötz, M. Carlen, Electrochim. Acta 45 (2000) 2483–2498.
[12] M.D. Stoller, S. Park, Y. Zhu, J. An, R.S. Ruoff, Nano Lett. 8 (2008) 3498–3502.
[13] S.-J. Bao, C.M. Li, C.-X. Guo, Y. Qiao, J. Power Sources 180 (2008) 676–681.
[14] S. Talapatra, S. Kar, S. Pal, K.R. Vajtai, L. Ci, P. Victor, M.M. Shaijumon, S. Kaur, O. Nalamasu, P.M. Ajayan, Nat. Nanotechnol. 1 (2006) 112–116.
[15] A.T. Chidembo, K.I. Ozoemena, B.O. Agboola, V. Gupta, G.G. Wildgoose, R.G. Compton, Energy Environ. Sci. 3 (2010) 228–236.
[16] G. Hodes, Chemical Solution Deposition of Semiconductor Films, Marcel Decker, New York, 2002.
[17] X. Xie, W. Shen, Nanoscale 1 (2009) 50–60.
[18] P. Benson, G.W.D. Briggs, W.F.K. Wynne-Jones, Electrochim. Acta 9 (1964) 275–280.
[19] F. Tao, Y.-Q. Zhao, G.-Q. Zhang, H.-L. Li, Electrochem. Commun. 9 (2007) 1282–1287.
[20] B. Liu, S. Wei, Y. Xing, D. Liu, Z. Shi, X. Liu, X. Sun, S. Hou, Z. Su, Chem. Eur. J. 16 (2010) 6625–6631.
[21] L. Cao, F. Xu, Y.-Y. Liang, H.-L. Li, Adv. Mater. 16 (2004) 1853–1857.
[22] M. Kaempgen, C.K. Chan, J. Ma, Y. Cui, G. Gruner, Nano Lett. 9 (2009) 1872–1876.
[23] Y. Xue, Y. Chen, M.-L. Zhang, Y.-D. Yan, Mater. Lett. 62 (2008) 3884–3886.
[24] Y. Wang, Z. Shi, Y. Huang, Y. Ma, C. Wang, M. Chen, Y. Chen, J. Phys. Chem. C 113 (2009) 13103–13107.
[25] H. Nakanishi, B.A. Grzybowski, J. Phys. Chem. Lett. 1 (2010) 1428–1431.
[26] J.R. McDonough, J.W. Choi, Y. Yang, F.L. Mantia, Y. Zhang, Y. Chi, Appl. Phys. Lett. 95 (2009) 243109–243112.